Available online at www.sciencedirect.com
ScienceDirect
Advances in Space Research 42 (2008) 712–719
ADVANCES IN SPACE RESEARCH (a COSPAR publication)
www.elsevier.com/locate/asr

Analysis of a topside ionospheric model using GPS and ionosonde observables

A. Meza [a,b,*], C. Brunini [a,b], A.E. Gularte Scarone [a,b], M. Mosert [b,c]

[a] Facultad de Ciencias Astronómicas y Geofísicas, Universidad Nacional de La Plata, Paseo del Bosque s/n, B1900FWA La Plata, Argentina
[b] Consejo Nacional de Investigaciones Científicas y Técnicas, Av. Rivadavia 1917, C1033AAJ Buenos Aires, Argentina
[c] Complejo Astronómico el Leoncito, C. de C. 467, 5400 San Juan, Argentina

Received 30 April 2007; received in revised form 10 August 2007; accepted 22 August 2007

Abstract

Ground-based vertical incidence soundings are well suited to model the bottom-side ionosphere but are not so good for dependably modelling the topside ionosphere. This study aims to combine vertical incidence sounding and dual-frequency GPS measurements to reconstruct the topside profile. The reconstruction technique relays on the use of the so-called vary-Chap approach that use an α-Chapman function with a continuously varying scale height.

We tested our technique with ionograms and GPS observations recorded at Ebro observatory, Spain (geomagnetic coordinates 43.6°N and 80.9°E). The contribution of the topside ionosphere to the vertical TEC was calculated as the difference between the vertical TEC estimated from GPS measurements and the contribution of the bottom-side ionosphere estimated by integration of the electron density obtained from ionograms. The obtained topside vertical TEC were used to estimate the parameters of the vary-Chap function that represents the topside profile, namely the transition height where the dominant ion species change from O^+ to H^+, the scale height at the transition height, and the shape factor that controls the steepness of the O^+ to H^+ transition.

The results are analyzed for solstices and equinoxes for a high solar activity year. The values obtained for the transition height are in agreement with those derived by other author. The topside profile seems to merge swiftly with an empirical plasmasphere model based on Radio Plasma Image measurements.

Keywords: Topside ionosphere; Total electron content; GPS; Ionosonde

1. Introduction

The representation of the electron density profile in the terrestrial atmosphere is widely studied thanks to sounding technologies. The traditional ground-based vertical incidence soundings determine the bottom-side electron density profile, i.e. the profile below the peak of the electron density distribution. To represent the topside profile, modern digital ionosondes use an α-Chapman layer model that depends on the peak parameters, i.e. the maximum electron density, N_mF_2, and the height of the peak, h_mF_2 (Reinisch, 1996; Reinisch and Huang, 2001). The main problems with this representation are the use of a constant scale height that is determined based on the measured density distribution around the peak, and that the constructed topside profile is not tied to any additional measurements.

Stankov et al. (2003) proposed a new method to reconstruct the topside profile by using GPS-TEC and vertical incidence sounding observations. In that work, the reconstructed topside profile is based on Chapman, sech-squared and exponential models, and the GPS-TEC is computed by using the calibration technique proposed by Sardon et al. (1994) in combination with the empirical model NTCM2 proposed by Jakowski et al. (1998). In this work

* Corresponding author. Address: Facultad de Ciencias Astronómicas y Geofísicas, Universidad Nacional de La Plata, Paseo del Bosque s/n, B1900FWA La Plata, Argentina. Tel.: +54 221 4236593; fax:+54 221 4236591.
E-mail address: ameza@fcaglp.unlp.edu.ar (A. Meza).

0273-1177/$34.00 © 2008 COSPAR. Published by Elsevier Ltd. All rights reserved.
doi:10.1016/j.asr.2007.08.042

we implemented the Stankov's procedure to asses the topside representation by means of a vary-Chap approach (Rishbeth and Garriot, 1969; Reinisch et al., 2007). In addition, GPS-TEC is calibrated by using the Ciraolo et al. (2007) technique.

The paper is organized in three main parts: first, we provide a short description of the procedure used to reconstruct the topside profile from GPS and vertical incidence sound measurements; then, we present the results obtained by applying that procedure to real data; and finally, we evaluate the obtained results and discuss the procedure herein applied.

2. Methodology

2.1. Parameterization of the topside electron density distribution

In order to reconstruct the topside profile, we use the vary-Chap approach proposed by Rishbeth and Garriot (1969), in which the topside electron density distribution is represented by an α-Chapman function with a height-varying scale height:

$$N_t(h) = N_m F_2 \cdot \left(\frac{H_m}{H(h)}\right)^{1/2} \exp\left\{\frac{1}{2}[1 - y(h) - \exp(-y(h))]\right\},$$
$$y(h) = \int_{h_m F_2}^{h} \frac{\mathrm{d}h'}{H(h')}, \tag{1}$$

where h is the height; $N_t(h)$ is the electron density distribution for the topside ionosphere; $H(h)$ is the height-varying scale height; and $H_m = H(h_m F_2)$ is the scale height at the F_2 peak.

Reinisch et al. (2007) used the available topside and plasmasphere electron density measurements to construct the scale height function. They conclude that a convenient form would be a hyperbolic tangent function:

$$H(h) = H_T + \frac{H_m - H_T}{\tanh(\beta)} \cdot \tanh\left(\beta \cdot \frac{h - h_T}{h_m F_2 - h_T}\right), \tag{2}$$

h_T being the transition height where the dominant ion species changes from O^+ to H^+; $H_T = H(h_T)$; and β being a shape factor that controls the steepness of the O^+ to H^+ transition.

Since $N_m F_2$, $h_m F_2$ and H_m can be computed from vertical incidence soundings (Huang and Reinisch, 1996), Eqs. (1) and (2) can be seen as the parameterization of the topside electron density distribution in terms of three unknown parameters, i.e. $N_t(h;H_T,h_T,\beta)$.

2.2. Link the unknown parameters to vertical incidence sounding and GPS measurements

In order to link the unknown parameters that define the topside electron distribution given by Eqs. (1) and (2) to vertical incidence soundings and GPS measurements, we split the vertical TEC ($vTEC$) in two contributions, one due to the bottom-side ionosphere ($bTEC$) and the other due to the topside ionosphere ($tTEC$), which allow us to write the following equation:

$$tTEC = \int_{h_m F_2}^{h_\infty} N_t(h; H_T, h_T, \beta) \cdot \mathrm{d}h = vTEC - bTEC, \tag{3}$$

h_∞ being the height where the electron density vanishes.

A value of the bottom-side contribution to $vTEC$ can be derived from vertical incidence soundings, since they provide the bottom-side electron density distribution as well as the height of the F_2 peak:

$$b\widetilde{TEC} = \int_0^{h_m F_2} \widetilde{N}_b(h)\mathrm{d}h, \tag{4}$$

where $\widetilde{N}_b(h)$ is the bottom-side electron density distribution derived by the thru-height inversion process applied to the critical frequencies and virtual heights measured by the sounder (Huang and Reinisch, 1996). The $vTEC$ can be derived from dual-frequency GPS measurements, as explained below.

The observation equation that relates the satellite-to-receiver slant TEC ($sTEC$) to the carrier-phase ionospheric observable, L_I, reads (Ciraolo et al., 2007):

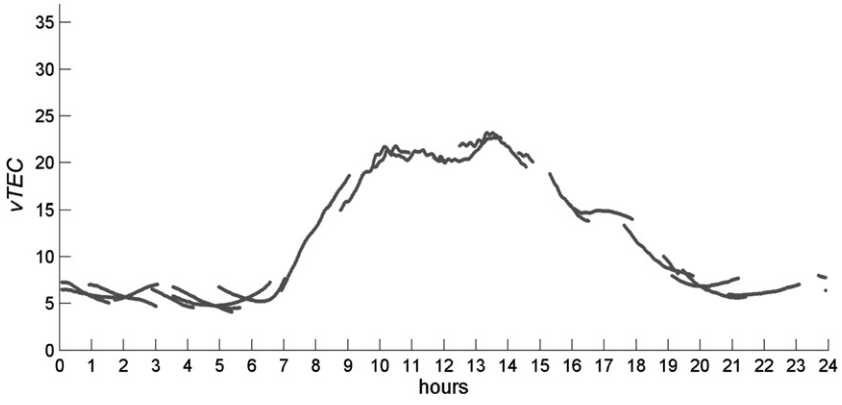

Fig. 1. Vertical total electron content ($v\widetilde{TEC}$) at Ebro observatory during a quiet geomagnetic day (only GPS observations with zenith distance lower than 25°).

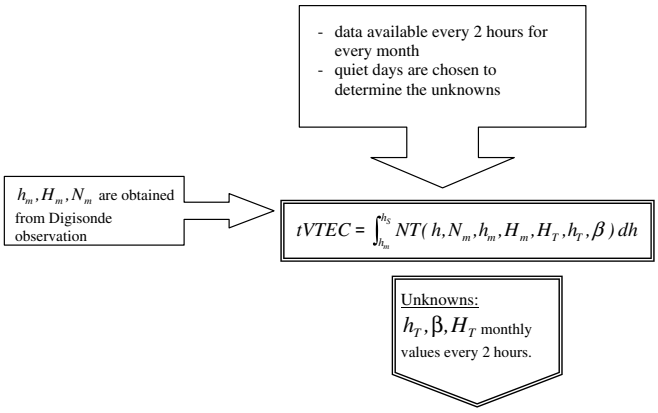

Fig. 2. Scheme of the parameter estimation process.

$$L_{\mathrm{I,arc}} = sTEC + b_{\mathrm{arc}} + \varepsilon_{L_\mathrm{I}}, \tag{5}$$

where the sub-index arc specifies a particular satellite arc; b_{arc} is the calibration bias that encompasses, all together, the inter-frequency satellite and receiver delays and the carrier-phase ambiguities; and $\varepsilon_{L_\mathrm{I}}$ is the observational and multi-path errors. In this context, a satellite arc means a group of consecutives observations that belong to the same satellite and are not affected by discontinuities. A widely used approach to estimate the calibration biases relays on the combination of carrier-phase and code-delay observations to reduce the effects of the carrier-phase ambiguities (Sardon et al., 1994). Once the ambiguities have been reduced, one inter-frequency bias is separately estimated for every satellite and for the receiver. Ciraolo et al. (2007) demonstrate that the estimation of an arc-dependent bias avoid the use of the code-delay and reduces calibration errors that are mostly due to code-delay multi-path.

Once the calibration biases have been estimated (as it will be immediately discussed), we can obtain calibrated $sTEC$ by a simple reduction of Eq. (5):

$$s\widetilde{TEC} = L_{\mathrm{I,arc}} - \tilde{b}_{\mathrm{arc}}, \tag{6}$$

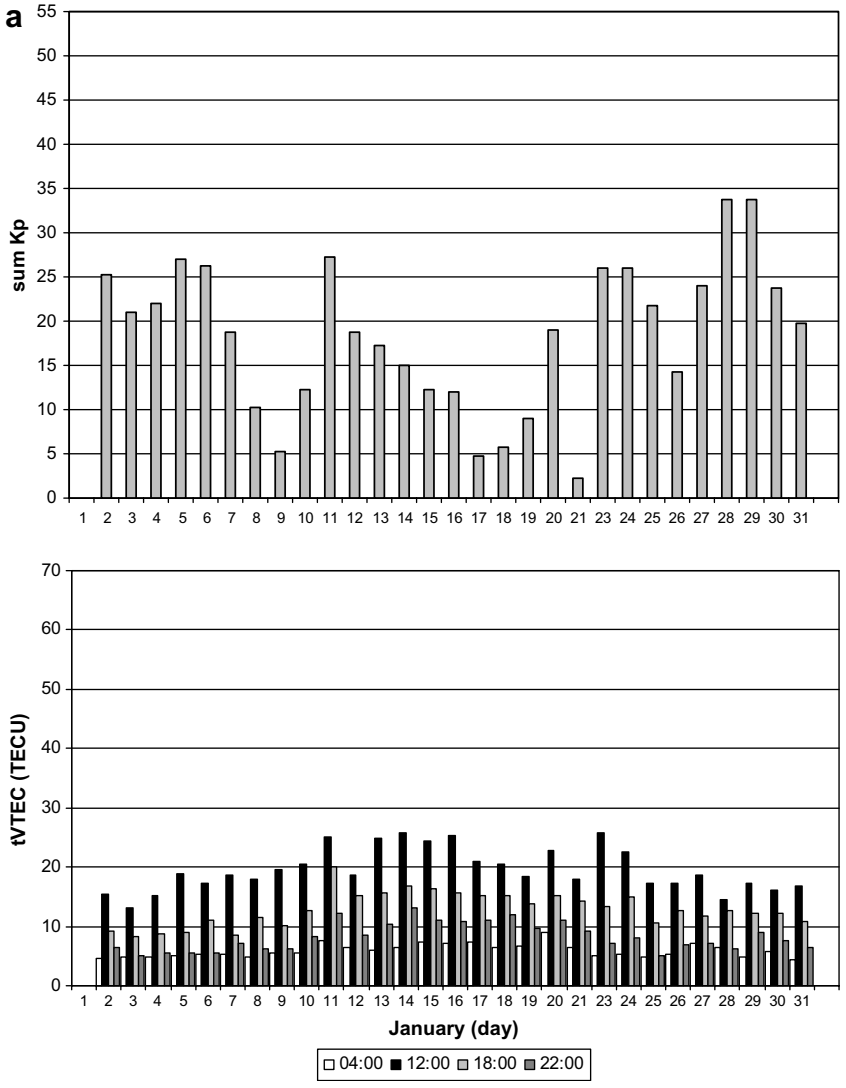

Fig. 3. The upper graph shows the geomagnetic activity recorded every day by Kp index and the bottom graph shows the topside contribution to the vertical TEC ($tT\widetilde{EC}$) obtained from vertical incidence soundings and GPS measurements (values in TECu) for (a) January, (b) July, (c) April and (d) October.

where $\tilde{b}_{\text{arc}}$ is the estimated bias. Further, the obtained $sT\widetilde{E}C$ is converted into $vT\widetilde{E}C$ by means of the thin-layer mapping function:

$$vT\widetilde{E}C = \cos z' \cdot sT\widetilde{E}C, \tag{7}$$

where z' is the zenith distance of the signal ray-path at the so-called piercing point. The piercing point is based on the so-called thin-shell approximation, which assumes that the ionospheric delay is produced by a spherical shell of infinitesimal thickness located close to the F_2 peak. The piercing point is the point where the signal pierces that shell.

In order to estimate the biases in Eq. (5), we represent the spatial variability of the $vTEC$ by using a bilinear expansion on the geographical longitude, λ and the latitude, φ, of the piercing point:

$$vTEC(\lambda, \varphi, t) = A(t) + B(t)(\varphi - \varphi_0) + C(t)(\lambda - \lambda_0), \tag{8}$$

where λ_0 and φ_0 are the geographical coordinates of the observing receiver. The temporal variability of the $vTEC$ is accounted for by the time-dependent coefficients, $A(t)$, $B(t)$ and $C(t)$, t being the Universal Time (UT) of the observation. The time-dependent coefficients are further expanded in trigonometrical polynomials with constant coefficients, e.g.:

$$A(t) = a_0 + a_1 \sin(wt) + b_1 \sin(wt) + a_2 \sin(2\,wt) + b_2 \times \sin(2\,wt) + \cdots, \tag{9}$$

where w is the one-per-day fundamental frequency.

The constant coefficients of the trigonometric polynomials and the calibration biases are jointly estimated from the carrier-phase ionospheric observations, in a daily basis and by applying the Least-Square method.

To provide an example, Fig. 1 shows the $vT\widetilde{E}C$ obtained by applying the previously described technique. It should be noted that there are cases in which two or more satellites are simultaneously located inside the circle of 25° around

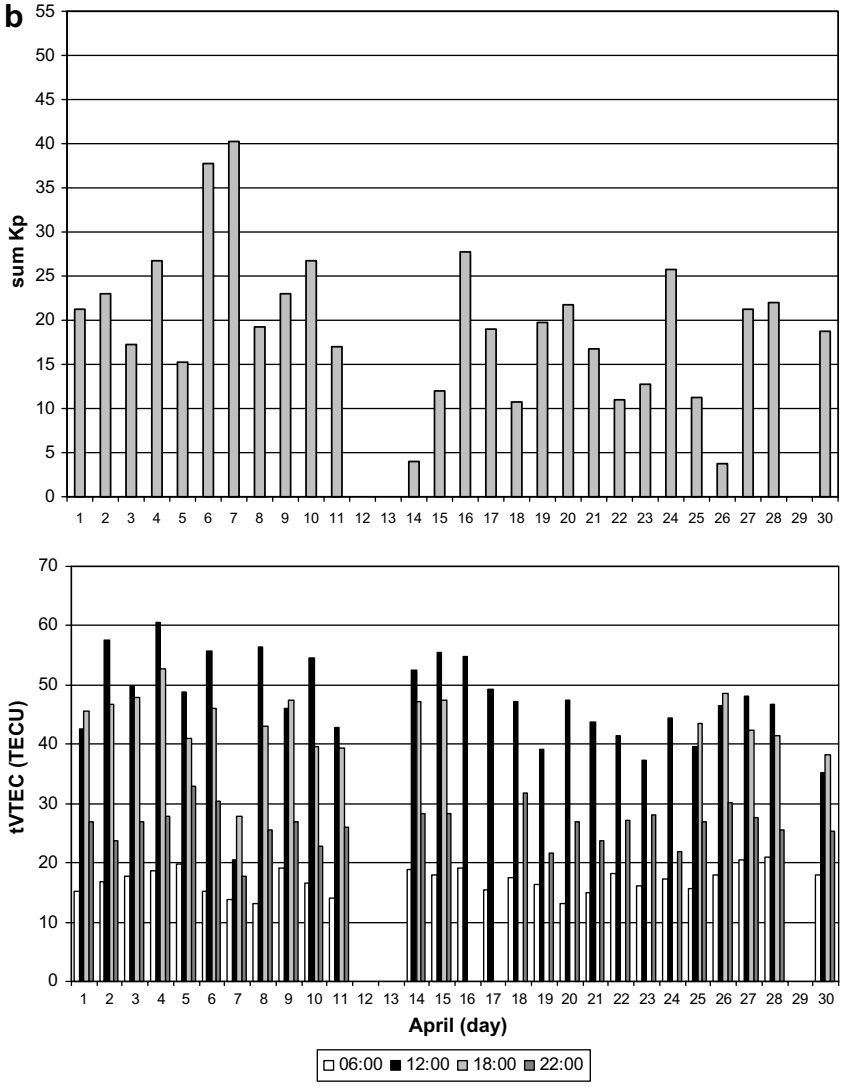

Fig. 3 (*continued*)

the zenith of the observing receiver. Due to their different locations, those satellites provide slightly different $vT\widetilde{E}C$ values for the same time. In this case, because the location of the observing receiver (43.6°N geomagnetic latitude), $vT\widetilde{E}C$ values from a satellite located to the South of the receiving station are higher than those from a satellite located to the North.

Now, we are able to re-write Eq. (1) in the following way:

$$tT\widetilde{E}C = vT\widetilde{E}C - bT\widetilde{E}C = \int_{h_mF_2}^{h_\infty} N_t(h; H_T, h_T, \beta) \cdot \mathrm{d}h + \varepsilon_{TEC} \quad (10)$$

where $vT\widetilde{E}C$ and $bT\widetilde{E}C$ have been obtained from the GPS measurements and the vertical incidence soundings, respectively, as previously discussed, and $\varepsilon_{\mathrm{TEC}}$ is the effect of the errors of both estimation techniques.

The unknown parameters in Eq. (10), i.e., H_T, h_T and β, are estimated by applying the Levenberg–Marquardt non-linear Least-Square method (Levenberg, 1944; Marquardt, 1963), as outlined in Fig. 2.

3. Results and discussion

The results presented in this section are based on ionograms and GPS observations recorded at Ebro, Spain (geomagnetic coordinates 43.6°N and 80.9°E). For this mid-latitude location, the ionospheric parameters that we are interested in behave in a rather predictable manner. Therefore, these results should be taken as a first attempt at tuning the technique. The study was undertaken for the year 2000 – a period with high solar activity ($F10.7 = 200$) – and covers solstice (January and July) and equinox (April and October) seasons.

Fig. 3a–d show the day-to-day variability of $tT\widetilde{E}C$ for each season and for different times of the day. The quiet and disturbed geomagnetic days can be identified by the sum of Kp index; it is plotted for every month in the same

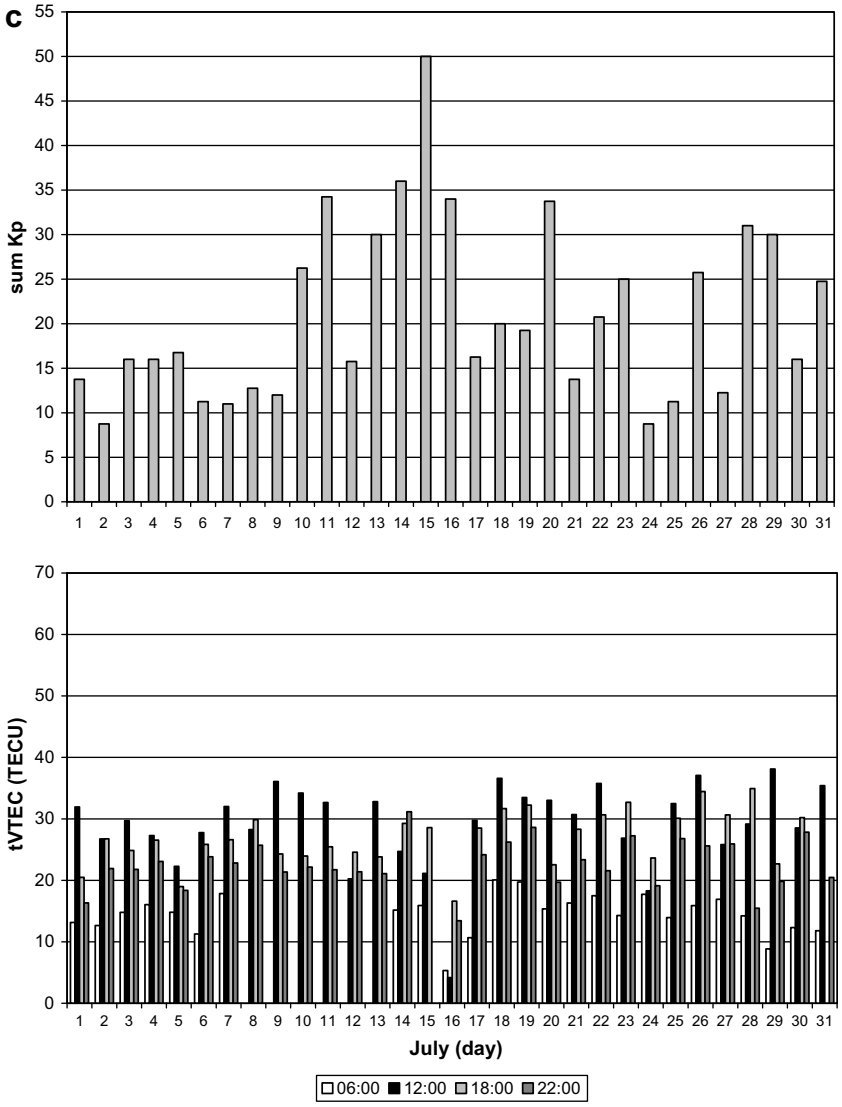

Fig. 3 (*continued*)

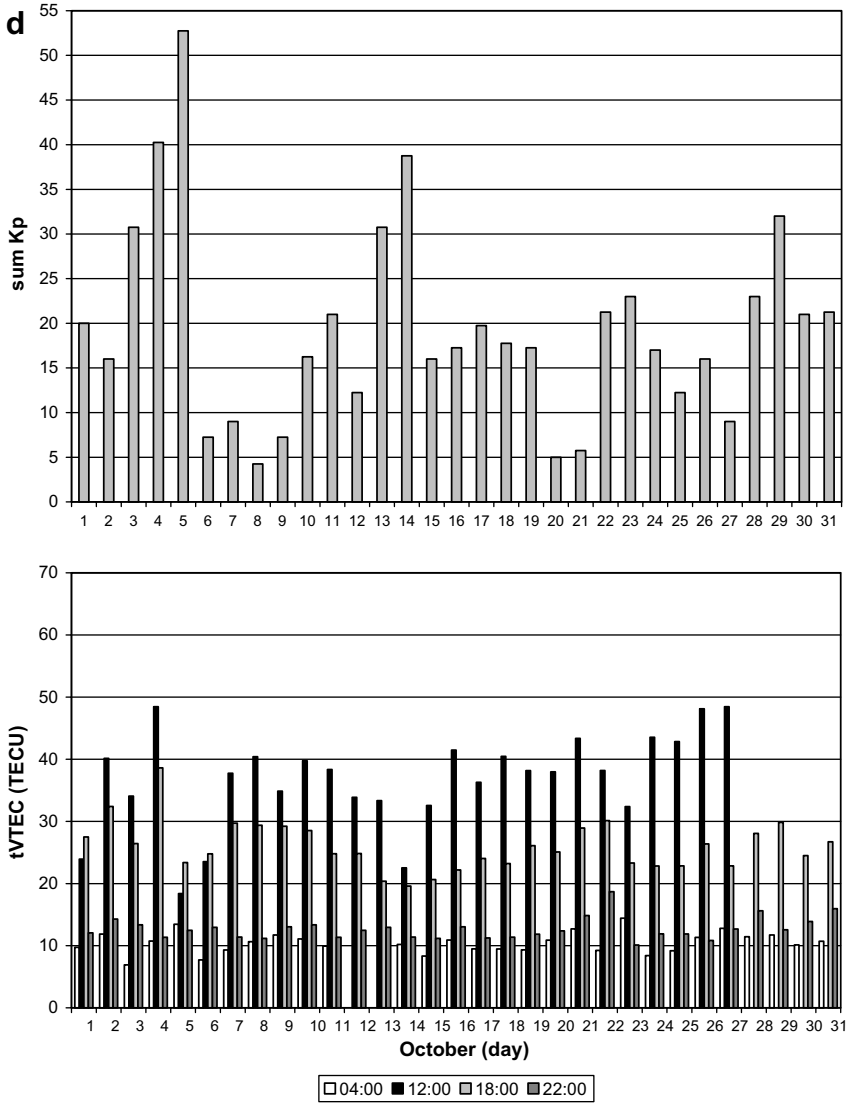

Fig. 3 (*continued*)

figure. The maximum values, around 60 TECu, are reached in April (spring in Northern Hemisphere) at 12:00 LT. The minimum values, lower than 10 TECu, are reached in January (winter in the Northern Hemisphere) during morning and night times. During quiet geomagnetic time, the day-to-day variability of $t\widetilde{TEC}$ is similar for each season, but during disturbed times, $t\widetilde{TEC}$ values can be significantly lower or higher than the quiet ones (e.g., on April 7 and 4 $t\widetilde{TEC}$ values are, respectively, higher and much lower than the monthly means). The abnormally low values that are observed for some disturbed days (e.g., January 14, April 7, July 16 and October 14) could be associated with the negative phase of an ionospheric storm.

The unknown parameters H_T, h_T and β have been estimated only for quiet geomagnetic days. Eq. (10) was solved for different 2-h intervals; therefore, the estimated parameters represent average values for these intervals. N_mF_2, h_mF_2 and H_m values were computed from the vertical incidence soundings. Fig. 4 presents the topside profile computed from Eq. (1), and the scale height computed from Eq. (2), for a 2-h interval centred on local noon, for the different seasons of the year (only one quiet geomagnetic day per season has been plotted). During the winter solstice, the topside profiles decay quicker than in the other seasons; correspondingly, the scale height is lower during winter solstice than during other seasons, being similar during summer solstices and autumn equinox. Table 1 shows that the transition heights estimated with our technique agree quite well with the mean values computed from the empirical model based on satellite measurements proposed by Kutiev et al. (1994). Fig. 5 shows that the topside profile computed from Eq. (1) merges swiftly with the plasmasphere profile computed with the plasma density model based on IMAGE/Radio Plasmasphere Imager (RPI) measurements (Reinisch et al., 2001; Huang et al., 2004).

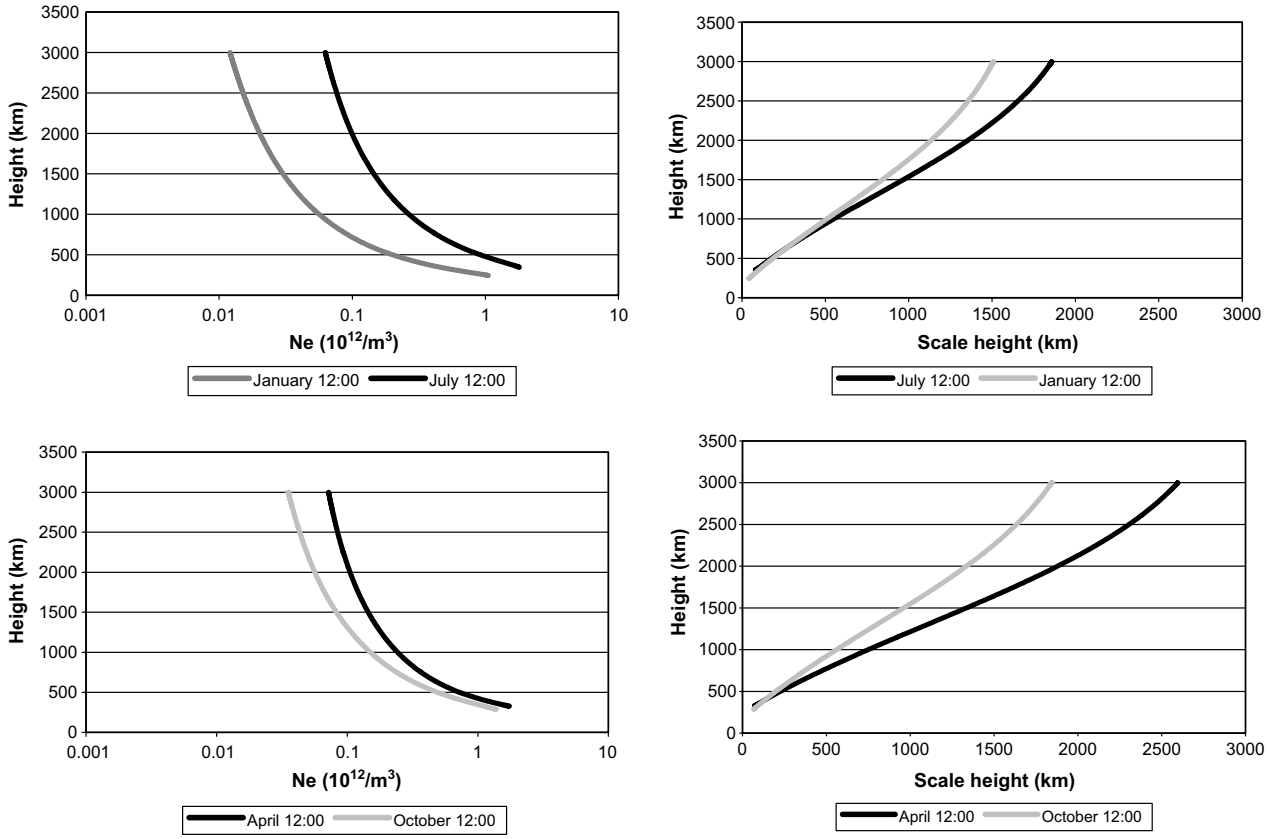

Fig. 4. Topside profiles in January and July (upper-right panel) and in April and October (bottom-right panel); scale height for the respective months (left panels).

Table 1
Transition height from and the corresponding mean values computed from the empirical model proposed by Kutiev et al. (1994)

	h_T (km)	h_T Kutiev (km)
Winter	830	1000
Spring	1300	1300
Summer	1300	1400
Autumn	1400	1300

4. Conclusions

This work proposes a reconstruction of the topside profile using the algorithms of Ciraolo et al., 2007 to obtain the *vTEC* from GPS observation. Similar to the methodology used by Stankov et al. (2003), the vary-Chap model is used here with three unknown parameters: h_T, β, H_T. We

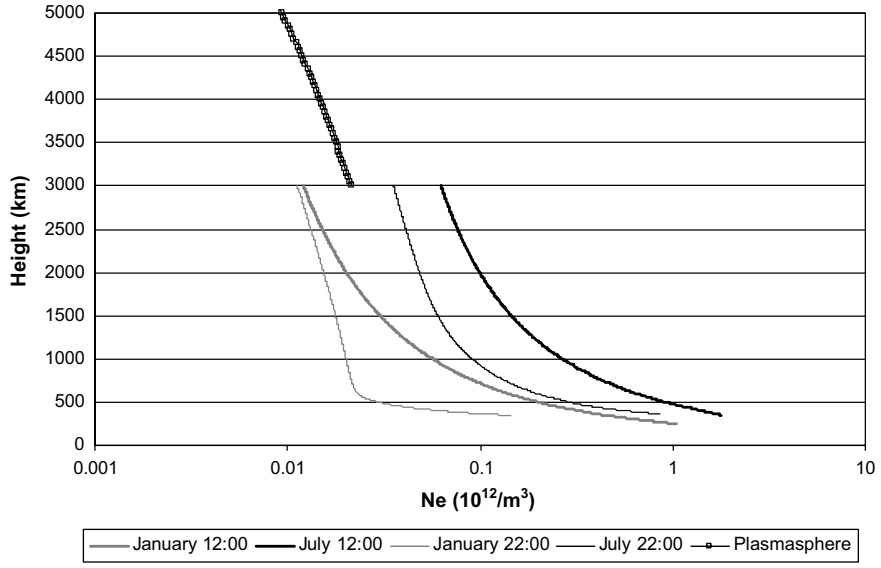

Fig. 5. Topside profiles for January and July at 12:00 and 22:00 LT and the modelled plasmasphere profile.

focus on seasonal variation at noon for maximum solar activity. The conclusion can be summarized as follows:

- The values of the upper transition level (h_T) are in agreement with those derived using other methods, and the average $NT(h)$ profile seems to merge swiftly with RPI density profiles.
- The reconstruction technique based on the vary-Chap model and GPS *vTEC* calibrated data has the potential of a reliable tool for ionospheric research.
- Measurements from other locations and by other type of observables will help to improve our topside profile. Using the observation generated by Ebro observatory, we are working on the analysis of profiles at different local time and in low and medium solar activity.

Acknowledgements

The authors are grateful to the ionospheric group at the Ebro observatory (Ebro, Spain) for providing the ionosonde data used in this study and to the Scripps Institution of Oceanography, University of California, San Diego, for providing the GPS data. This work was supported with grants from the Universidad Nacional de La Plata and the Consejo Nacional de Investigaciones Científicas y Técnicas, Argentina.

References

Ciraolo, L., Azpilicueta, F., Brunini, C., Meza, A., Radicella, S.M. Calibration errors on experimental slant total electron content determined with GPS. J. Geodesy 81 (2), 111–120, 2007.

Huang, X., Reinisch, B.W., Song, P., Green, J., Gallager, D. Developing and empirical density model of plasmasphere using IMAGE/RPI observations. Adv. Space Res. 33 (6), 829–832, 2004.

Huang, X., Reinisch, B.W. Vertical electron density profiles from the digisonde network. Adv. Space Res. 18 (6), 21–29, 1996.

Jakowski, N., Sardon, E., Schlueter, S. GPS-based TEC observations in comparison with IRI95 and the European TEC model NTCM2. Adv. Space Res. 22 (6), 803–806, 1998.

Kutiev, I., Stankov, S.M., Marinov, P. Analytical expression of O^+–H^+ transition surface for use in IRI. Adv. Space Res. 14 (12), 135–138, 1994.

Levenberg, K.A. Method for the solution of certain non-linear problems in least squares. Quart. Appl. Math. 2, 164–168, 1944.

Marquardt, D. An algorithm for least-squares estimation of nonlinear parameters. SIAM J. Appl. Math. 11, 431–441, 1963.

Reinisch, B.W., Huang, X., Song, P., Sales, G.S., Fung, S.F., Green, J.L., Gallagher, D.L., Vasyliunas, V.M. Plasma density distribution along the magnetospheric field: RPI observations from IMAGE. Geophys. Res. Lett. 28, 4521–4524, 2001.

Reinisch, B.W., Huang, X. Deducing topside profiles and total electron content from bottomside ionograms. Adv. Space Res. 27 (1), 23–30, 2001.

Reinisch, B.W. Ionosonde, in: Dieminger, G., Hatmann, H., Leitinger, R. (Eds.), The Upper Atmosphere – Data Analysis and Interpretation. Springer-Verlag, New York, pp. 370–381, 1996.

Reinisch, B.W., Nsumei, P., Huang, X., Bilitza, D.K. Modeling the F2 topside and plasmasphere for IRI using IMAGE/RPI and ISIS data. Adv. Space Res. 39 (5), 731–738, 2007.

Rishbeth, O.K., Garriot, H. Introduction to Ionospheric Physics. Academic Press, New York, 1969.

Sardon, E., Rius, A., Zarraoa, N. Estimation of the transmitter and receiver differential biases on the ionospheric total electron content from Global Positioning System observations. Radio Sci. 29, 577–586, 1994.

Stankov, S.M., Jakowski, N., Heise, S., Muhtarov, P., Kutiev, I., Warnant, R. A new method for reconstruction of the vertical electron density distribution in the upper ionosphere and plasmasphere. J. Geophys. Res. 108 (A5), 1164, doi:10.1029/2002JA009570, 2003.